The Effect of the Strain Rise Phenomenon on the Deformation Capacity

of Concentric Braces

Hassan Moghaddam[1], Ali Sadrara[2], Mohammadreza Saji[3]

[1] *Professor, Sharif University of Technology, moghadam@sharif.edu*
[2] *PhD candidate, Sharif University of Technology, ali.sadrara@student.sharif.edu*
[3] *Graduated, Sharif University of Technology, mrsaji86@gmail.com*

Abstract

The paper presents the results of an investigation on the strain rise caused by the occurrence of local buckling in concentric steel braces during earthquakes. It is demonstrated that this phenomenon predominates the fracture failure, and therefore, should be considered as the relevant index for evaluating the deformation capacity of bracing members. A series of concentric steel braces models are subjected to the loading cycles of increasing amplitude, and the occurrences of global and local bucklings are captured using nonlinear FE analyses, calibrated and verified against experimental tests. The results show that the overall buckling is generally followed by the occurrence of local buckling at mid-span. At this stage, the geometry changes radically, and some singularity regions develop, resulting in the formation of an intense strain concentration. This is designated as The Strain Rise Phenomenon, and is responsible for the unexpected premature failure of the concentric braces in earthquakes. The results indicate that once the local buckling occurs, the strains at the critical region rise exponentially with the loading cycles, and they soon become many hundred times greater than the yield strain. It is also demonstrated that the rupture can be evaluated adequately by Finite Element Analysis (FEA) considering the strain rise at the critical region, and using the Cyclic Void Growth Model (CVGM). A comparison of the results with the experiments indicates on reasonable accuracy. A comprehensive study is conducted on various braces. The results are used to check the accuracy of the collapse levels suggested by the existing standard codes such as ASCE 41-17. It is concluded that the suggested collapse levels can sometimes become erroneous as the code do not take into account the effect of the local buckling explicitly, and rather rely solely upon the overall buckling. Alternative relationships are suggested for evaluating the axial deformation capacity of the steel braces taking into account the thickness to width ratio which controls the strain rise phenomenon caused by the local buckling.

Keywords: Strain-Rise; Fracture life; Local buckling; Strain concentration; CVGM model

1. Introduction

Braced frames are one of the most common lateral load resisting systems. The stability of these structural system is highly dependent on the deformation capacity of the brace. Fracture of the brace is a threat for the stability of the whole structure. Therefore, evaluation of the parameters which affect the deformation capacity and fracture behavior is of most importance. Many researchers investigated the behavior of the brace and they tried to find a way to improve the behavior of this structural system [4-15].

During earthquakes brace and its connections experience large-amplitude cyclic loading. Therefore, these structural component must have sufficient deformation capacity and energy absorbing. If the connections are designed properly, at first, global buckling occurs and load carried by the brace decreases [1]. Then, in large-amplitude cyclic loading, two ends and the middle of brace yield. As the cyclic loading continues, local buckling and localization of plasticity at the midpoint leads to a sharp increase in plastic strain with a high rate. Therefore, premature fracture occurs in the brace. This premature fracture is a consequence of a phenomenon called as Strain Rise. In essence strain rise is defined as a sharp, unexpected and progressive increase in equivalent plastic strain of steel components that have concentration in their stress field. Existence of holes, cracks or notches in a structural component causes stress concertation which tremendously reduces the ductility and deformation capacity due to disturbance in the stress and strain field. This reduction of ductility is the direct result of strain rise that is evaluated in this study. In structural engineering over the past decades, stress concentration was not considered as a highly problematic issue. Because beyond linear state, due to the redistribution of the stresses, the strength of structures is not affected significantly. Therefore, in design codes, stress concentration effects are neglected. In structures, in light of the fact that steel can endure large plastic strains prior to fracture and its high ductility, it is assumed that stress concentration does not threat the stability of structure and it is fracture safe. Beyond the elastic state, strain in critical points like notch roots, rise up swiftly and drastically with a high rate. This drastic growth in strain leads to premature fracture.
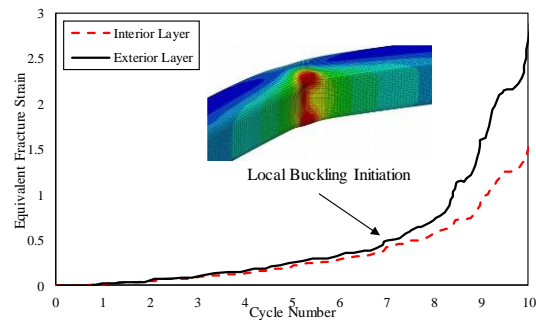

(a)

(b)

(c)

(d)

2
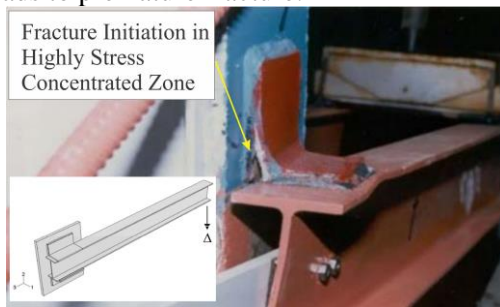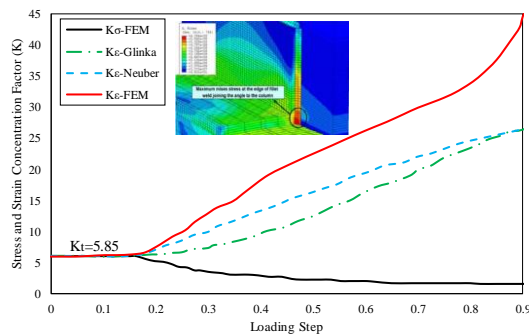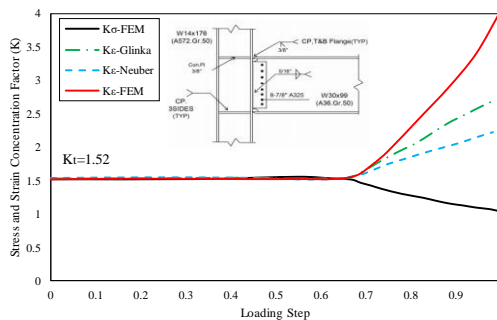
Fig. 1 – strain rise examples: (a) Khorjini connection (b) strain rise in fillet weld of Khorjini connections (b) strain rise in pre-Northridge connections (c) strain rise in braces after local buckling

In Manjil earthquake (1990) widespread premature fracture in Khorjini connection was observed. Several numerical and experimental studies were conducted by the first author on this type of connections afterward. Fig. 1-a shows one of these experiments and process of the loading. The fracture mode observed in the test was similar to the one which was observed in earthquake. Numerical studies showed that the fracture initiated in the highly stress concentrated zone. The K_σ (stress concentration factor) and K_ε (strain concentration factor) of the point where crack initiates against loading steps are plotted in Fig. 1-b. This plot shows that K_σ and K_ε in the elastic regime are the same and equal to 5.85. At the beginning of yielding, K_σ tends to decrease while the K_ε increases sharply which results in the initiation of crack. The predicted value of K_ε of Neuber's and Glinka's formulations during loading process are presented.

In Northridge earthquake (1994) several connections experienced unexpected and premature fracture. One of these connections was Welded Unreinforced Flange (WUF). In these connections most of the cracks initiated in complete joint penetration weld between beam flange and column flange shown in Fig. 1-c. This plot shows K_σ and $K\varepsilon$ against loading steps in the aforementioned weld. The same pattern as Fig. 1-b can be observed in this graph where after yielding the unexpected increase in plastic strain leads to premature fracture.

Fig. 1-d shows the von Mises equivalent plastic strain (denoted as ε_p hereafter) of interior and exterior layer of a HSS brace in the middle of its length subjected to cyclic loading. At first, ε_p of the interior and exterior layers are the same but when local buckling initiates, interior and exterior ε_p begin to bifurcate. Growth of ε_p occurs after local buckling initiation. This phenomenon which leads to premature fracture of the brace is another example of strain rise.

1.1 Cyclic Void Growth Model (CVGM)

In order to identify the fracture instant during a cyclic loading, CVGM is used which is the cyclic form of the Void Growth Model (VGM) [3]. They derived the relation between stress state and void growth for a single spherical void in an elastic perfectly plastic space as follows

$$\frac{dR}{R_0} = 0.283 \exp\left(\frac{1.5\sigma_m}{\sigma_y}\right) d\varepsilon_p \tag{1}$$

In which σ_m, ε_p and R are mean stress (hydrostatical dilatation stress), increment of von Mises plastic strain and R is the radius of void, respectively. Increment of von Mises equivalent plastic strain and stress triaxiality are written as

$$d\varepsilon_p = \sqrt{\frac{2}{3} d\varepsilon_{ij} d\varepsilon_{ij}} \tag{2}$$

$$T = \frac{\sigma_m}{\sigma_e} \tag{3}$$

$$\sigma_e = \sqrt{\frac{3}{2} s_{ij} s_{ij}} \tag{4}$$

In which σ_e is von Mises or distortional stress and s_{ij} are the components of deviator stress tensor. Integrating both sides of Eq.1 and substitution of Eq.3 in Eq.1 results in

3

$$\ln\left(\frac{R}{R_0}\right) = 0.283 \int_0^{\varepsilon_p} \exp(1.5T) d\varepsilon_p \tag{5}$$

Void Growth Index (VGI) is a parameter which is defined as

$$VGI = \frac{\ln\left(\dfrac{R}{R_0}\right)}{0.283} = \int_0^{\varepsilon_p} \exp(1.5T) d\varepsilon_p \tag{6}$$

It is assumed that in monotonic loading fracture occurs at VGI_{cr}^{mono} or in other words if the demand VGI reaches VGI_{cr}^{mono} fracture occurs. VGI_{cr}^{mono} is defined as

$$VGI^{mono} = \int_0^{\varepsilon_p} \exp(|1.5T|) d\varepsilon_p \tag{7}$$

CVGM is the cyclic form of the VGM which considers the effect of tensile and compressive load excursions.

In this model the demand parameter is defined as

$$VGI^{cyclic} = \sum_{tensile} \int_{\varepsilon_1}^{\varepsilon_2} \exp(|1.5T|) d\varepsilon_p^t - \sum_{tensile} \int_{\varepsilon_1}^{\varepsilon_2} \exp(|1.5T|) d\varepsilon_p^c \tag{8}$$

In which ε_p^t and ε_p^c are tensile and compressive plastic strain, respectively. The critical value of void growth index, due to the damage of the material as a result of cyclic loading is less than that of monotonic loading. This decrease is presented in exponential form as

$$VGI_{cr}^{cyclic} = \exp(-\lambda\xi) VGI_{cr}^{mono} \tag{9}$$

$$\xi = \sum \varepsilon_p^c \tag{10}$$

Fracture occurred whenever the demand parameter exceeds the capacity or in the other words, $VGI^{cyclic} > VGI_{cr}^{cyclic}$.

2. Description of the specimens

In this study 23 cyclic tests conducted by [4-6] are modeled and verified. Therefore, the result of the present study is supported by experimental data which makes the results more reliable. Specimens No.1 to 4, No.5 to 14 and No.15 to 23 are based on the experiments of references [4], [5] and [6], respectively. The dimensions and geometries of the braces are presented in Table 1. Fig. 2 shows a schematic view of the braces.
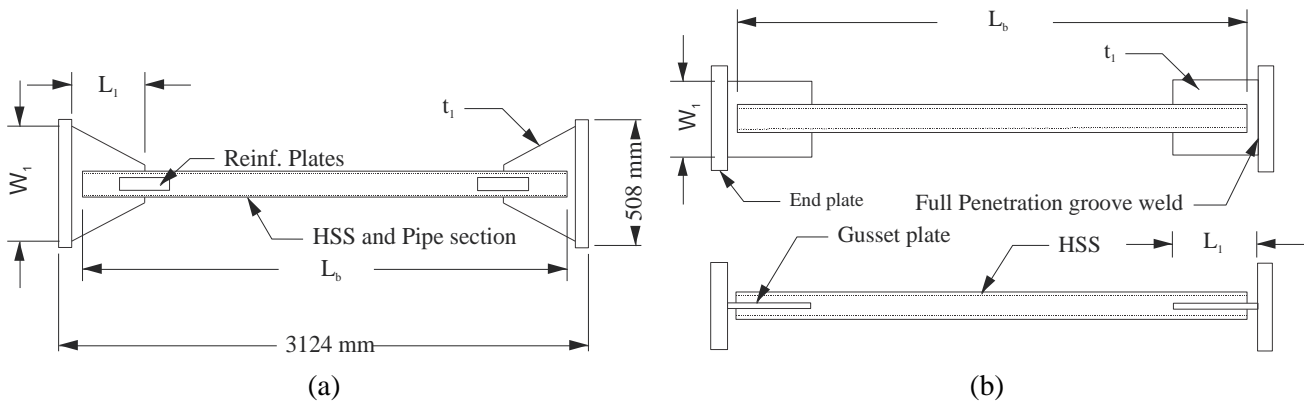
Fig. 2 - The geometry of the specimens of (a) reference [4] and (b) references [5], [6]

Table 1 – The geometry of the braces

			BRACES							GUSSET PLATE			
No	SEC.	b×d×t	R*	L_b	KL_b/r	b/t or D/t	Fy (Mpa)	E (Gpa)	L_1	W_1	t_1	free length
1	HSS1	101.6×101.6×6.4	15	3022	0.77	10.83	468	200	292	508	12.7	38
2	HSS2	101.6×101.6×9.5	20	3022	0.80	6.76	441	200	419	508	12.7	38
3	Pipe1	141.22×6.45	-	3048	0.55	21.89	379	200	343	508	12.7	38
4	Pipe2	88.9×5.48	-	3048	0.89	16.20	351	200	203	508	12.7	38
5	HA-1	152×152×8	20	4950	0.65	13.00	467	200	350	250	25.4	50
6	HA-2	152×152×8	20	4950	0.65	13.00	467	200	350	250	25.4	50
7	HA-3	152×152×8	20	4950	0.65	13.00	467	200	350	250	25.4	50
8	HA-4	127×127×8	20	4450	0.66	9.88	480	200	300	225	25.4	50
9	HA-5	127×127×8	20	4450	0.54	9.88	480	200	300	225	38.1	50
10	HA-6	127×127×8	20	4450	0.50	9.88	480	200	300	225	50.8	50
11	HA-7	127×127×8	20	3150	0.50	9.88	480	200	300	225	25.4	50
12	HA-8	127×127×13	20	4450	0.68	5.69	500	200	300	350	25.4	50
13	HA-9	127×127×13	20	4450	0.52	5.69	500	200	300	350	50.8	50
14	HA-10	127×127×13	20	3550	0.52	5.69	500	200	300	350	25.4	50
15	1A	127×127×6.4	15	3450	0.52	14.16	461	196	300	200	25.4	50
16	1B	127×127×8	18	3450	0.54	10.38	421	191	300	225	25.4	50
17	2A	152×152×8	18	4050	0.53	13.50	442	202	350	250	25.4	50
18	2B	152×152×9.5	19	4050	0.52	11.00	442	196	350	300	25.4	50
19	3A	127×127×6.4	15	4450	0.65	14.16	461	196	300	200	25.4	50
20	3B	127×127×8	18	4450	0.66	10.38	421	191	300	225	25.4	50
21	3C	127×127×9.5	20	4450	0.62	8.16	461	202	300	250	25.4	50

5

| 22 | 4A | 152×152×8 | 18 | 4950 | 0.64 | 13.50 | 442 | 202 | 350 | 250 | 25.4 | 50 |
| 23 | 4B | 152×152×9.5 | 20 | 4950 | 0.60 | 10.79 | 442 | 196 | 350 | 300 | 25.4 | 50 |

*Corner radius

The specimens in references [4], [5] and [6] are subjected to the load protocols presented in Fig. 3-a, Fig. 3-b and Fig. 3-c, respectively. It is worth noting that the load protocol of reference [4] is a far field load protocol and taken from the corrected standard load protocol of ATC for braced frames.
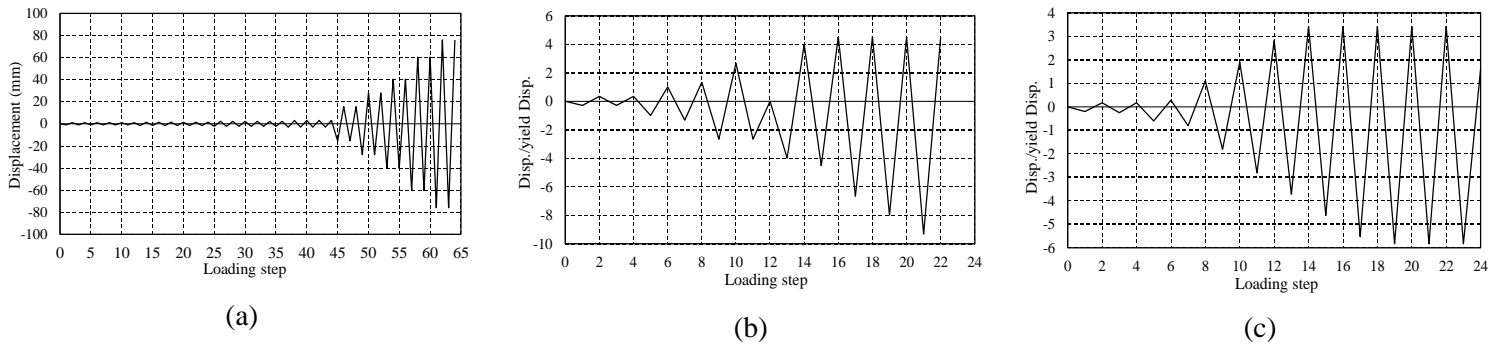

(a)   (b)   (c)

Fig. 3 - Load protocols applied to the specimens of (a) reference [4] (b) reference [5] (c) reference [6]

3. Fracture and local buckling analysis

In order to model the behavior of braces, commercial FE software (ABAQUS) is used [22]. Due to symmetric boundary conditions and loading, only ¼ of the brace is modeled which reduces the computational cost considerably. In FEA, 4-node shell element with reduced integration (S4R) is used. In order to properly capture the local buckling and fracture instant, 5 integration point are used through the thickness of the brace. To specify an appropriate mesh size, a mesh dependency analysis shown in Fig. 4 is performed on Pipe 1. As shown, mesh size of 1mm seems to be suitable for plastic strain analysis. Therefore, Mesh size is chosen as 1mm×1mm in the middle of the brace and 5mm×1mm in the other parts.
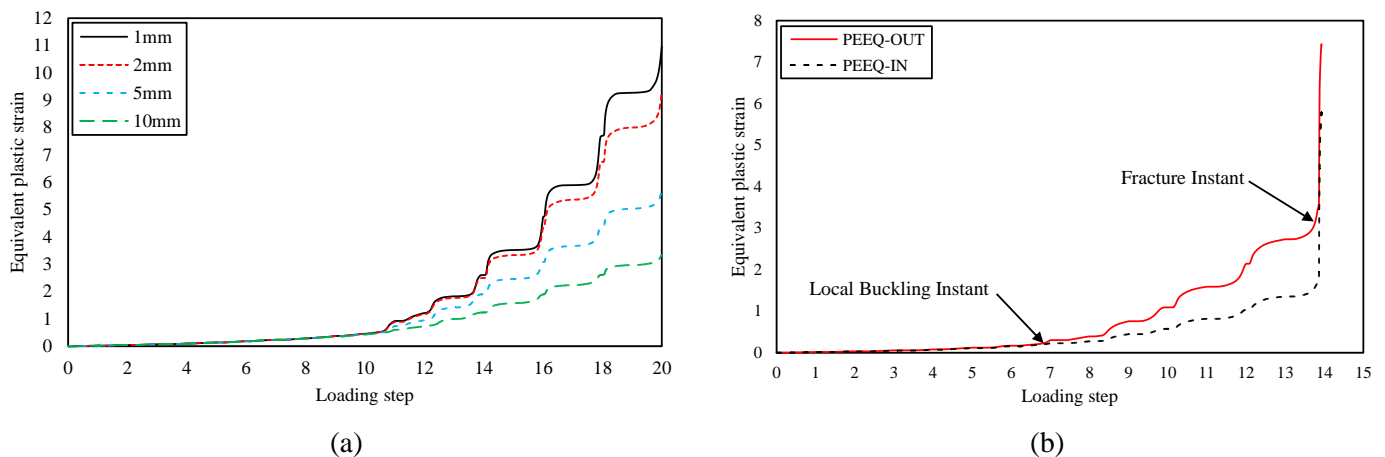

(a)   (b)

Fig. 4 - (a) Mesh dependency of the equivalent plastic strain (b) Equivalent plastic strain of inner and outer layer and in HSS 1 specimen

3.1 Spotting local buckling and fracture

The step at which the strain of the inner layer diverges from the outer layer of a section, identifies the occurrence of the local buckling. To detect the local buckling, the plastic strain of the inner and outer layer at the critical point in the middle of the brace is plotted in Fig. 4 for HSS 1. As shown, the local buckling and

6

the fracture occur at loading step 7 and 14, respectively. The results of the analyses indicate that local buckling occurs in compression and the plastic strain increases sharply. Although local buckling occurs in the compression, the brace fails in tension. In order to detect the critical (fracture initiation) point of the section in the middle of the brace, it is necessary to track the growth of plastic strain in different angles on the periphery of the brace. The plane of gusset plates is defined as 0° and 180° angle. Fig. 5-a and b shows the plastic strain distribution of Pipe 1 and HSS 1, respectively. As shown, the maximum plastic strain occurs in the angle of 40° to 50° for both braces similar to the experimental fracture loci.

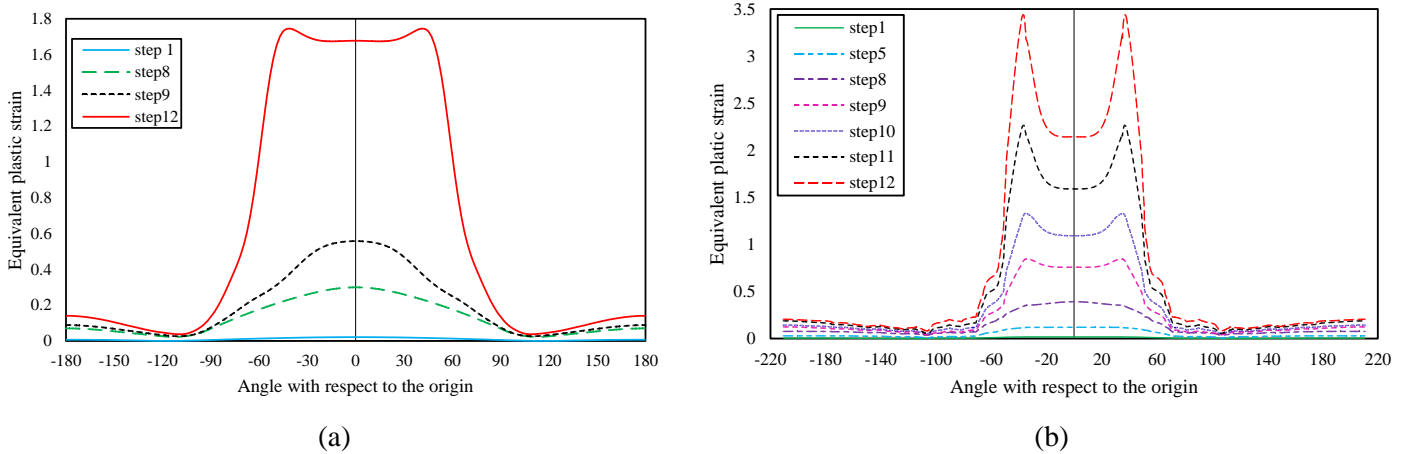(a)   (b)

Fig. 5 - Equivalent plastic strain distribution in (a) Pipe 1 and (b) HSS 1 braces

After finding the critical point, fracture prediction analysis based on CVGM is conducted on the brace. Fracture index parameter is defined as

$$FI = \frac{VGI^{cyclic}}{VGI_{cr}^{cyclic}} \tag{11}$$

Whenever the FI parameters reaches unity fracture occurred. The process of fracture prediction of HSS 1 is presented in Fig. 6.

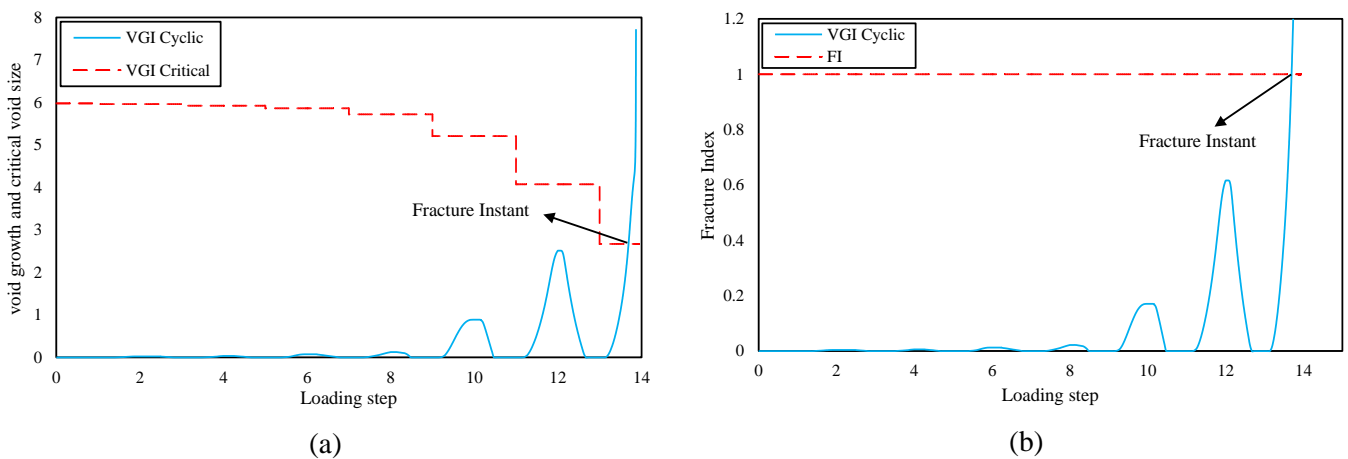(a)   (b)

Fig. 6 - Prediction of fracture initiation in HSS1 section (a) VGI (b) FI approaches

Local buckling and fracture instant are calculated using above-mentioned method. Fig. 7-a compares the experimental and FEA local buckling instant and indicates that FEA have a good accuracy. Fracture instant of FEA and experiment is also compared in Table 2. for the specimens of references [4] and [5]. A good

7

agreement between experimental results and that of FEA is observed. It is worth noting that fracture did not occur in some specimens.

Table 2 - Comparison of local buckling and fracture instant in experiment and FEA [4] [5]

SEC	Fracture FEM	Fracture EXP
HSS1	7	6
HSS2	NA*	12
Pipe3	NA*	14
Pipe5	7	6
HA-1	9	10
HA-2	8	9
HA-3	8	9
HA-4	9	9
HA-5	8	9
HA-6	8	7
HA-7	7	8
HA-8	NA*	22
HA-9	NA*	18
HA-10	NA*	18

*NA: The fracture instant was not reported by the author

The instant of the local buckling and fracture initiation of some specimens are presented in Table 3. As indicated, there is a slight difference between local buckling and fracture initiation instants. This is due the fact that, after occurrence of local buckling the plastic strain in critical point rises abruptly and it induces premature fracture in a few cycle. Therefore, the local buckling instant can be considered as a limit state in the design of the steel braces.

Table 3 – Comparison of local buckling and fracture loading cycle in FEA

SEC	local buckling FEM	Fracture FEM
1A	7	8
1B	8	9
2A	7	8
2B	8	9
3A	8	9
3B	10	NA*
3C	12	NA*
4A	8	9
4B	9	11

*NA: the specimen did not experience fracture

3.2 Fracture life

In this section, effective parameters on the fracture life of the brace is evaluated. The most important parameter is the local slenderness (b/t or D/t). Another effective parameter is yield stress indicated by [6]. Many studies are presented relations to find the fracture of the braces [5, 6], [14-16]. Although these relations are rather rough, it makes the calculations simpler without the need for FEA. To quantify the fracture life of a brace, normalized cumulative fracture displacement is defined as

$$\Delta_F^{demand} = \sum_{loading} \frac{\left(\left|\Delta_c^b\right| + \Delta_t^b\right)}{\Delta_{GB}} \tag{12}$$

In which Δ_F^{demand} and Δ_{GB} are the demand normalized cumulative fracture displacement and global buckling displacement, respectively. Δ_c^b and Δ_t^b are the displacements of compressive and tensile load excursion, respectively. The displacements of the brace from global buckling to fracture instant are summed to represent deformation capacity of the brace.

In this study a relation is proposed to predict the fracture instant of the HSS and Pipe braces. This relation is calibrated by the experimental results. Therefore, the capacity normalized cumulative fracture displacement is calculated as

$$\Delta_F^{capacity} = \frac{1}{C_s}\left(\frac{b}{t}\right)^{-0.9}\left(\frac{KL_b}{r}\right)^{2.4}, C_s = 51.5 \tag{13}$$

Whenever the demand normalized cumulative fracture displacement exceeds the capacity normalized cumulative fracture displacement the fracture is assumed to be occurred. In Fig. 7-b the fracture instants predicted by Eq. (12) is compared to those of experimental data and a good agreement can be observed.

3.3 ASCE 41-17 code

According to ASCE 41-17 [25] steel braces, based on their global slenderness, are fallen into three distinct categories, slender, intermediate and stocky braces. In each category, the deformation capacity of the brace is calculated for different performance level. The limitations of the code are based on the global buckling displacement in compression and yielding displacement in compression. In order to evaluate the limitation of the code, in Fig. 7-c the displacement corresponded to local buckling is compared to the Collapse Prevention (CP) and Life Safety (LS) limits. As shown, code limitations failed to predict the local buckling instant. It can be due to the fact that the code limitations do not consider the local slenderness, while the deformation capacity of the brace highly depends on local slenderness. Furthermore, the limitations of the code do not consider the effect of cyclic loading which is a commonplace load protocol in earthquakes.
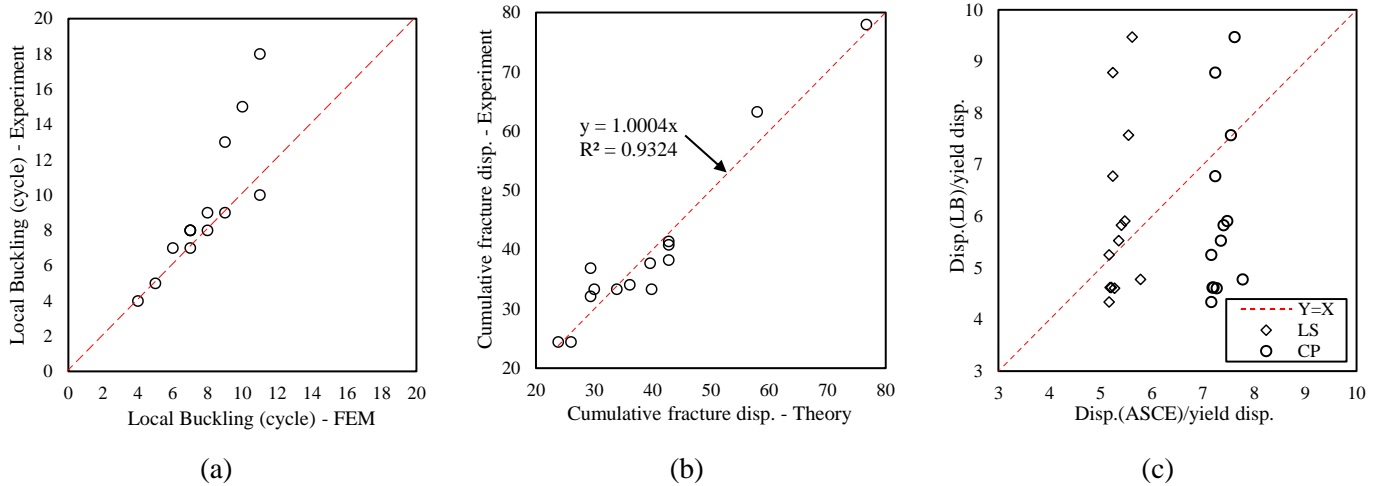
Fig. 7 - Comparison of (a) experimental vs. FEA local buckling instant (b) experimental vs. Theoretical normalized cumulative fracture displacement (c) FEA vs. ASCE Normalized local buckling instant

4. Conclusion

In this study, 23 specimens which were tested by previous researches [4-6] were modeled. The local buckling instant of the braces are calculated using a simple approach. In addition, the fracture instant of the braces are predicted using CVGM. The calculated local buckling and fracture instants are verified against experimental results. It is shown that fracture occurs immediately after local buckling instant. Therefore, local buckling can be considered as a limit state. A relation is proposed to calculate the cumulative fracture displacement based on experimental results. The limits of the ASCE 41-17 for LS and CP were compared to the values of FEA and a considerable difference was observed. The reason is that code limits are based on the global behavior of the braces and do not consider the local stability proved to be a very important parameter in fracture life. Choosing the displacement, which is corresponding to the local buckling of the brace, as a limit state results in a good safety threshold.

6. References

[1] Zaredasjerdian, M. (2010). Evaluation of the performance of braced frames (MSc dissertation). Sharif University of Technology, Tehran, Iran.

[2] Fell, B. V., Kanvinde, A. M., Deierlein, G. G., & Myers, A. T. (2009) Experimental Investigation of Inelastic Cyclic Buckling and Fracture of Steel Braces. Journal of Structural Engineering, 135(1), 19–32.

[3] Kanvinde, A. M., & Deierlein, G. G. (2004). Micromechanical Simulation of Earthquake Induced Fractures in Steel Structures, Blume Center TR145.

[4] Fell, B. V., Kanvinde, A. M., & Deierlein, G. G. (2010). "Large scale testing and simulation of earthquake induced ultra-low cycle fatigue in bracing members". Department of Civil and structural Engineering, Stanford University: The John A. Blume Earthquake Engineering Research Center, No. 172

[5] Haddad, M., Brown, T., & Shrive, N. (2011). Experimental cyclic loading of concentric HSS braces. Canadian Journal of Civil Engineering, 38(1), 110–123.

[6] Shaback, B., & Brown, T. (2003). Behavior of Square Hollow Structural Steel Braces with End Connections Under Reversed Cyclic Axial Loading. Canadian Journal of Civil Engineering, 30(4), 745–753.

[7] Astaneh - Asl, A., & Goel, S. C. (1984). Cyclic In - Plane Buckling of Double Angle Bracing. Journal of Structural Engineering, 110(9), 2036‑ 2055.

2b-0129

[8] Tremblay, R., Archambault, M.-H., & Filiatrault, A. (2003). Seismic Response of Concentrically Braced Steel Frames Made with Rectangular Hollow Bracing Members. Journal of Structural Engineering, 129(12).

[9] Elchalakani, M., Zhao, X.-L., & Grzebieta, R. (2003). Tests of Cold-Formed Circular Tubular Braces under Cyclic Axial Loading. Journal of Structural Engineering, 129(4), 507–514.

[10] Han, S.-W., Kim, W. T., & Foutch, D. A. (2007). Seismic Behavior of HSS Bracing Members according to Width–Thickness Ratio under Symmetric Cyclic Loading. Journal of Structural Engineering, 133(2), 264–273.

[11] Takeuchi, T., & Matsui, R. (2011). Cumulative Cyclic Deformation Capacity of Circular Tubular Braces under Local Buckling. Journal of Structural Engineering, 137(11), 1311–1318.

[12] Haddad, M., Brown, T., & Shrive, N. (2011). Finite element modeling of concentric HSS braces under cyclic loading. Canadian Journal of Civil Engineering, 38(5), 493–505.

[13] Kuşyılmaz, A., & Topkaya, C. (2011). A numerical study on local buckling and energy dissipation of CHS seismic bracing. Thin-Walled Structures, 49(8), 984–996

[14] Tang, X., & Goel, S. C. (1989). Brace Fractures and Analysis of Phase I Structure. Journal of Structural Engineering, 115(8).

[15] Lee, S. and Goel, S.C. 1987. Seismic behavior of hollow and concrete-filled square tubular bracing members. Report No. UMCE87-11, Department of Civil Engineering, The University of Michigan, Ann Arbor, Michigan.

[16] Archambault, M.H. 1995. Etude du comportement seismique des contreventements ductiles en X avec profiles tubulaires en acier .Report No EPM/GCS-1995-09 . Department of Civil Engineering, Ecol Polytechnique, Montreal

[17] Tremblay, R., Archambault, M.-H., & Filiatrault, A. (2003). Seismic Response of Concentrically Braced Steel Frames Made with Rectangular Hollow Bracing Members. Journal of Structural Engineering, 129(12).

[18] Astaneh - Asl, A., Goel, S. C., & Hanson, R. D. (1985). Cyclic Out - of - Plane Buckling of Double - Angle Bracing. Journal of Structural Engineering, 111(5), 1135‑ 1153.

[19] CSA. CAN/CSA-S16.1-94. (1994). Limit states design of steel structures. Rexdale, Ont: Canadian Standard Association.

[20] Lee, K., & Bruneau, M. (2005). Energy Dissipation of Compression Members in Concentrically Braced Frames: Review of Experimental Data. Journal of Structural Engineering, 131(4), 552–559.

[21] Panontin, T. L. and Sheppard, S.D, (1995) The relationship between constraint and ductile fracture initiation as defined by micromechanical analyses. Fracture Mechanics: 26 Volume. ASTM STP 1256

[22] Abaqus, Inc. (2014). Abaqus/CAE User's Manual.

[23] American Institute of Steel Construction (AISC). (2016). Seismic Provisions for Structural Steel Buildings - ANSI/AISC 341-16, Chicago.

[24] Federal Emergency Management Agency. (2000). Pre-standard and Commentary for the Seismic Rehabilitation of Buildings: FEMA-356.

[25] ASCE/SEI Seismic Rehabilitation Standards Committee. (2017). Seismic Rehabilitation of Existing Buildings (ASCE/SEI 41-17). American Society of Civil Engineers, Reston, VA.

11